

The impact of exponentially varying viscosity on magnetized tangent hyperbolic nanofluid over a nonlinear stretching sheet with PHF and PMF conditions

Mohamed Magdy Ghazy^{1,2}, Khalid Saad Mekheimer^{1*}, Rabea Elshennawy Abo-Elkhair^{3,1} and Ahmed Mostafa Megahed⁴

¹ Department of Mathematics, Faculty of Science (Men), Al-Azhar University, **Egypt**


² Department of Mathematics, German International University (GIU), **Egypt**

³ Department of Basic Science, October High Institute of Engineering Technology-OHI, **Egypt**

⁴ Department of Mathematics, Faculty of Science, Benha University, **Egypt**

* Corresponding Author: Kh_mekheimer@azhar.edu.eg

Received: 17 February 2025; 1st Revised: 08 May 2025; 2nd Revised: 22 May 2025; Accepted: 26 May 2025

 Cite this <https://doi.org/10.24036/teknomekanik.v8i1.33772>

Abstract: This article aims to explore the characteristics of tangent hyperbolic nanofluid flow over a nonlinear exponentially stretching sheet with suction or injection embedded in a Darcy porous medium. We consider a non-Newtonian magnetohydrodynamic fluid with prescribed surface temperature and temperature-dependent viscosity, relevant to applications in aerospace, automotive and marine engineering, electronic cooling, solar-energy systems, and filtration. Given its fundamental importance, the study of prescribed exponential order heat flux (PHF) and prescribed mass flux (PMF) of hyperbolic tangent nanofluid became a key in research aimed at improving the efficiency and performance of these systems. The partial differential equations are converted into ODES by using transformation procedure. The system of transformed equations is numerically solved by Chebyshev spectral method. Graphical results illustrate the impact of key parameters on concentration, velocity, and temperature profiles, while tabulated data report the local Nusselt number, Sherwood number, and skin friction coefficient. Our results show that increasing both the power-law index and the variable-viscosity parameter reduces the fluid's velocity while elevating its temperature and concentration. The comparative analysis confirms a high degree of agreement with previous studies. This research holds significant importance as it focuses on the extensive utilization of tangent hyperbolic nanofluids in cooling electronic components that produce substantial heat during their operation.

Keywords: tangent hyperbolic nanofluid; variable heated viscosity; exponential stretching sheet; PHF and PMF; Chebyshev spectral method

1. Introduction

In the chemical engineering field, the tangent hyperbolic rheological model is preferred over the traditional Newtonian model which describes fluid behavior with a linear stress-strain relationship. The tangent hyperbolic model outperforms other non-Newtonian formulations in terms of computational effectiveness, practical utility, and robustness [1]. Additionally, it is deduced from the liquid kinetic theorem, as opposed to empirical relation. No known model can encompass the entire spectrum of non-Newtonian fluids characteristics. Several non-Newtonian models are used to illustrate non-Newtonian fluids, one of which is the tangent hyperbolic model [2]. One of the first researchers in this field was Sakiadis [3], who studied how a boundary layer flows across a continuously solid surface at a constant speed. Crane [4] developed the concept and characterized the viscous fluid resulting in a smooth stretched surface with a linear velocity variation. Discovering an equivalent solution is the most fascinating aspect of the investigation. Wang [5] studied the laminar flow of unsteady viscous fluid, and similarity solutions to the governing equation were

obtained. Non-Newtonian fluid across stretching surfaces and using the shooting method for getting a numerical solution to the governing equation was discussed by Cortell [6]. Malik et al., [7] presented the numerical solutions of tangent hyperbolic nanofluid under the influence of MHD through a stretching cylinder by applying the Keller box method. Researcher-produced material on boundary layer flows over stretched sheets can be found in references [8], [9], [10].

Since non-Newtonian boundary layer fluid through a stretching surface has many different industrial uses, including polymers, textiles, food processing, and so on, it had been the focus of the research for a long time. Non-Newtonian fluids are more commonly used in modern manufacturing than Newtonian fluids [11]. These additions can enhance fluid performance expanding the range of applications. In every manufacturing process, the quality of the finished product is greatly influenced by the rate of cooling during heat transfer operations. Magnetohydrodynamics (MHD) is one of the variables that will be utilized for determining the outcome of the desired attribute and assessing the rate of cooling. Alali and Megahed [12] introduced an MHD Casson nanofluid film flow as a result of an unstable stretching surface with radiation effect and the slip velocity, and magnetic field phenomenon. The magneto-hydrodynamics flow of a hybrid nanofluid (Ag-CuO/H₂O) through a permeability stretched surface porous medium with magnetic field, suction/injection, and multiple slips impacts was explained by Yahaya et al., [13]. Shahzad et al., [14] demonstrated the MHD of Jeffery nanofluid flow over a permeable stretched sheet besides viscous dissipation and heat generation influences. Abbas et al., [15] simulated the thermal conductivity of Maxwell nanofluid with magnetic field impacts on a vertically stretched sheet across the porous medium. Vitta et al., [16] reported the numerical study of the boundary layer MHD of a Sisko nanofluid through a permeability stretched surface using Runge-Kutta fourth-order scheme. The MHD effects in a 3D flow for suspended nanofluids (Cu-water/methanol) through stretching surface were discussed by Akber et al., [17]. Nabwey et al., [18] had provided heat transfer in 2D of Carreau ternary-hybrid nanofluid flow with MHD through an exponential stretched of a curve surface. Naveed et al., [19] has considered hydro-magnetic of couple stress fluid flow over a porous stretchable oscillatory sheet with heat transfer in the presence of homogeneous and heterogeneous chemical reactions. Existing studies [20], [21], [22], [23] performed the boundary layer flow on stretched sheet by using Newtonian and non-Newtonian nanofluids, at elevated temperature and various physical conditions.

A nanofluid consists of nanometer-sized particles dispersed in a conventional base fluid, improving the combined heat and mass transfer processes. This innovation emerged after decades of experimental research aimed at overcoming the poor thermal conductivity of traditional heat transfer fluids. Previous attempts, including flow geometry modifications and addition of micro- or milli-sized particles, proved ineffective. The nanotechnology approach successfully addressed these limitations, leading to widespread applications across multiple industries. Today, nanofluids play crucial roles in electronics cooling, automotive systems, refrigeration, renewable energy (solar heaters and fuel cells), nuclear power, and various thermal management applications, marking a significant advancement in heat transfer technology. Choi [24] introduced the first mention of nanofluids in 1995. Scientists and engineers can now conduct study in a new field thanks to this trial. Bounghiorno et al., [25] discovered nanofluid applications for nuclear reactors and they made the argument that nanofluids are more advantageous economically and for nuclear reactor safety than their base fluid counterparts. Wang and Mujumda [26] examined the studies on nanofluids by numerous researchers. They pointed out that it is extremely difficult to theoretically predict the thermo-physical characteristics of nanofluids based on observations of thermal conductivity, viscosity, etc. The nanofluid flow of the boundary layer through the stretching sheet were firstly discussed by Khan and Pop [27]. They discovered that the model used for the nanofluid includes Brownian motion and that thermophoresis effects are important. Hayat et al., [28] has investigated the effects of mixed convection, thermophoresis, and Brownian motion on the MHD boundary layer of thixotropic nanofluid flow. Ferdows et al., [29] studied numerical solution for the

incompressible boundary layer flow of nanofluid with porous medium and heat generation and viscous dissipation effects over a moving plate. Reddy and Sreedevi [30] presented the thermal radiation of nanofluid across an inclined plate with a porous medium, chemical reaction and solved numerically using the finite element method. Awati et al., [31] discussed heat transfer of the boundary layer of nanofluid moving over a permeable stretched surface and solved numerically by using the Chebyshev collocation method. Maiti and Mukhopadhyay [32] considered magnetic impacts on a boundary layer flow of hybrid nanoliquid through a divergent porous channel. Many researchers have studied boundary layer flows of Newtonian and non-Newtonian nanofluids through stretching sheets under various thermal and physical conditions [33], [34], [35], [36], [37]. However, these cited studies primarily focused on constant viscosity and lacked a comprehensive analysis of the combined effects of magnetic fields, variable viscosity, and realistic boundary conditions such as prescribed heat flux (PHF) and prescribed mass flux (PMF). Our study directly addresses these limitations by incorporating these critical factors into the investigation.

In addition to the significance of a magnetic field in heat transfer and boundary layer flow, viscous dissipation is included in the energy equation. The energy source and viscous dissipation both play important roles in altering temperature distribution and, consequently, heat transfer rate [38]. Applications for this process include the processing of polymers and the ducting of oil products. Viscosity dissipation's impact on natural convection was initially studied by Gebhart [39]. He came to the conclusion that viscous dissipation could not be ignored in a natural convection flow of a fluid with a high Prandtl number or a flow subject to strong gravitational forces. Following that, studies on the impact of viscous dissipation were conducted because of its uses in the lubrication, power generation, and plasma physics sectors, among other industries. Cortell [40] discussed the viscous dissipation effect and variable surface temperature on viscous flow over a stretching sheet. The impact of viscous and ohmic dissipation on the MHD boundary layer flow of a viscoelastic fluid over a stretching sheet was examined by Abel et al., [41]. Ramandevi et al., [42] investigated the effects of the viscous dissipation on MHD non-Newtonian fluid flow with Cattaneo-Christov heat flux. Recently, Anitha et al., [43] studied the entropy generation for non-Newtonian tangent hyperbolic fluid in a microchannel under effect non-linear thermal radiation. Other advancements in this area have been explored through significant investigations by esteemed researchers [44], [45], [46].

A noticeable gap in the literature exists regarding the combined influence of exponentially varying viscosity, magnetic field effects, and non-standard boundary conditions such as prescribed heat and mass flux (PHF and PMF) on the flow behavior of tangent hyperbolic nanofluids. While previous studies have explored aspects of non-Newtonian nanofluid flow, they have not sufficiently addressed the interplay between variable viscosity, magnetic fields, Brownian motion, and suction/injection effects in such configurations. To model these transport phenomena accurately, the present study adopts the Buongiorno model, which focuses on Brownian motion and thermophoresis as dominant mechanisms in nanofluid transport, without considering the explicit size of nanoparticles. This study aims to fill the identified gap by analyzing the complex interactions of these parameters over a nonlinear stretching surface. The incorporation of exponentially temperature-dependent viscosity provides a more realistic model, and the use of the Chebyshev spectral method allows for accurate simulation of the governing flow dynamics.

In real-world applications like biomedical fluid dynamics, where precise predictions of fluid behavior around biological structures or in medical devices are critical, understanding the flow dynamics driven by variable viscosity and specific boundary conditions (PHF and PMF) is key [47], [48]. These discoveries can help improve fluid-based system efficiency and safety in industrial and medical settings by optimizing design parameters.

2. Material and methods

Newtonian fluids display a straightforward flow where their viscosity remains constant regardless of how fast they are sheared. In contrast, non-Newtonian fluids, like the tangent hyperbolic nanofluid in this research, show a more complex behavior where their viscosity decreases as the shear rate increases. This characteristic makes them particularly well-suited for simulating intricate flow patterns in cutting-edge engineering applications. In addition, the governing equations are solved numerically using the Chebyshev collocation method (CCM). This method is a very precise numerical technique for solving differential equations, especially effective for boundary layer problems with smooth solutions. It works by approximating the solution using Chebyshev polynomials and solving the equations at specific Chebyshev–Gauss–Lobatto collocation points. This method offers several benefits, such as exponential convergence, the ability to provide a global approximation, and efficient handling of boundary conditions. Because it can accurately capture steep changes with fewer data points, it's particularly well-suited for nonlinear and non-Newtonian fluid flow problems, like those found in nanofluid dynamics over stretching surfaces.

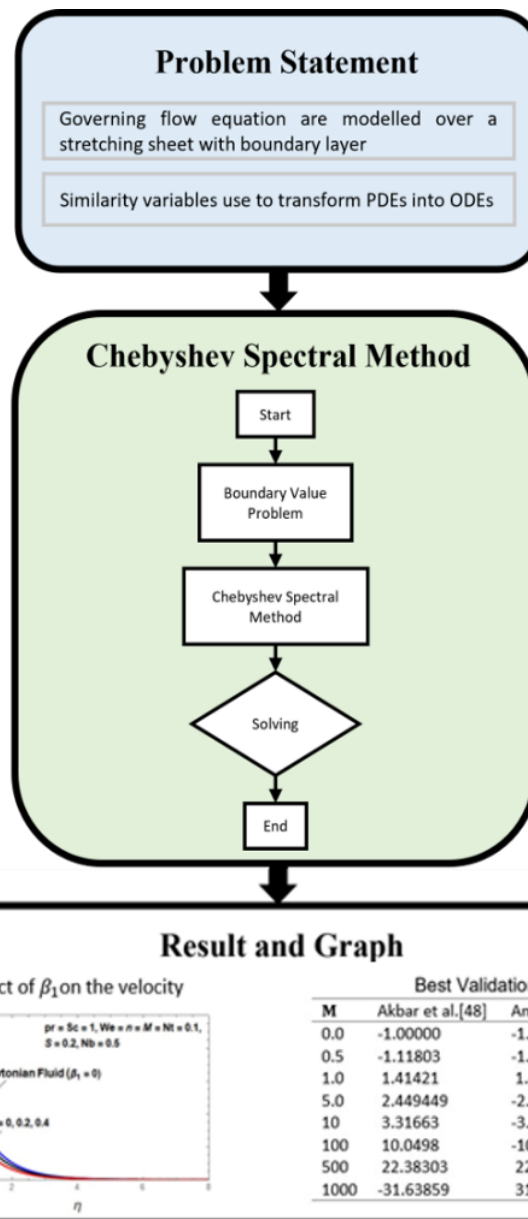


Figure 2. Flow chart of methodology applied

Before delving into the flowchart, we need to detail the numerical procedure used to solve the converted system of equations. This flowchart visually maps out the computational steps, from transforming the equations to applying the Chebyshev spectral method and finally obtaining the numerical solutions. This guide ensures readers can easily follow the methodology and grasp the solution approach. The numerical workflow is summarized as follows:

1. **Start:** Initialize the boundary value problem (BVP) derived from the transformed ODEs.
2. **Boundary Value Problem:** Define boundary conditions for the exponential stretching sheet.
3. **Chebyshev Spectral Method:**
 - Discretize the domain using Chebyshev collocation points on $[-1,1]$
 - Convert the ODEs into algebraic equations via spectral differentiation matrices.
4. **Solving:** Numerically solve the system using iterative or direct solvers.
5. **End:** Extract solutions (velocity profiles, shear stress) and validate against benchmarks.

2.1 Mathematical model and formulation

We investigated the non-Newtonian boundary layer of tangent hyperbolic nanofluid flow through an exponentially nonlinear stretching surface, solved numerically using the Chebyshev spectral method, as illustrated in Figure 1, with the flow confined to the region $y > 0$. At the wall ($y = 0$), the sheet is stretched in the x -direction with velocity $u_w = A_0 e^{\frac{x}{l}}$, accompanied by a suction/injection velocity, a prescribed heat-flux (PHF) condition, and a prescribed mass-flux (PMF) condition. A variable transverse magnetic field $B = B_0 e^{\frac{x}{2l}}$ is applied along the y -axis. The fluid motion arises from the opposing action of two parallel forces. The wall temperature and ambient temperature are denoted by T_w and T_∞ , respectively, while C_w and C_∞ represent the nanoparticle concentration at the wall and in the ambient fluid.

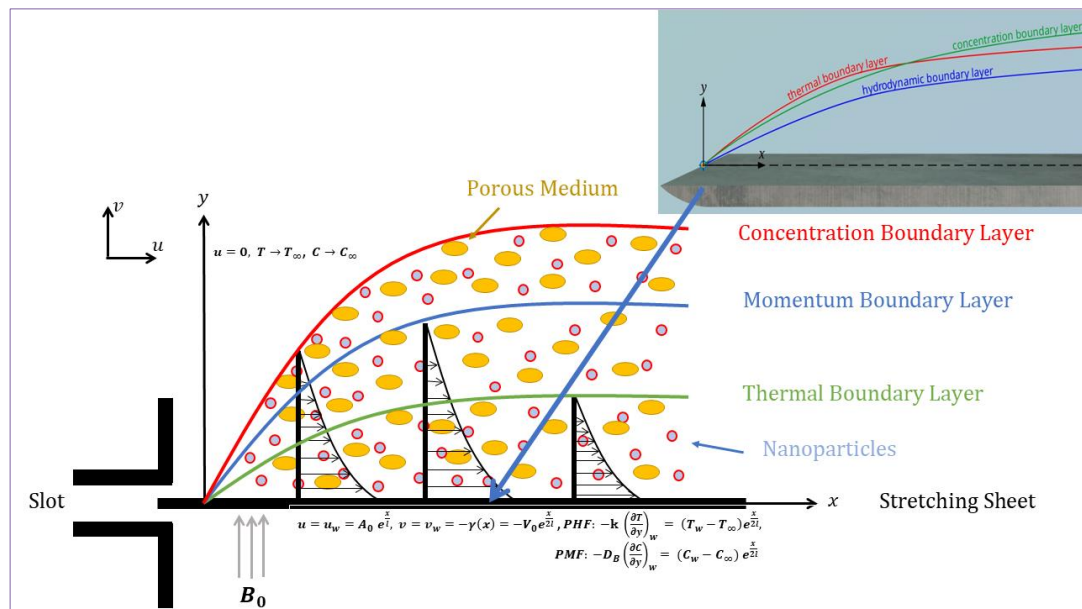


Figure 2. Sketch of physical problem

The fundamental boundary layer equations are described as [49], [50]:

$$\frac{\partial u}{\partial x} + \frac{\partial v}{\partial y} = 0, \quad (1)$$

$$u \frac{\partial u}{\partial x} + v \frac{\partial u}{\partial y} = \frac{1}{\rho} \frac{\partial}{\partial y} (\mu(1-n) \left(\frac{\partial u}{\partial y}\right) + \frac{\mu \Gamma n}{\sqrt{2}} \left(\frac{\partial u}{\partial y}\right)^2) - \frac{\sigma B_0^2}{\rho} u, \quad (2)$$

$$u \frac{\partial T}{\partial x} + v \frac{\partial T}{\partial y} = \frac{\rho_p c_p}{\rho c} [D_B \frac{\partial C}{\partial y} \frac{\partial T}{\partial y} + \frac{D_T}{T_\infty} \left(\frac{\partial T}{\partial y}\right)^2] + \alpha \frac{\partial^2 T}{\partial y^2}, \quad (3)$$

$$u \frac{\partial C}{\partial x} + v \frac{\partial C}{\partial y} = D_B \frac{\partial^2 C}{\partial y^2} + \frac{D_T}{T_\infty} \frac{\partial^2 T}{\partial y^2}, \quad (4)$$

We assume that the boundary conditions are the following [49], [50]:

$$\left. \begin{aligned} u = u_w = A_0 e^{\frac{x}{l}}, \quad v = v_w = -\gamma(x) = -V_0 e^{\frac{x}{2l}}, \\ PHF: -k \left(\frac{\partial T}{\partial y}\right)_w = (T_w - T_\infty) e^{\frac{x}{2l}}, \\ PMF: -D_B \left(\frac{\partial C}{\partial y}\right)_w = (C_w - C_\infty) e^{\frac{x}{2l}} \text{ when } y = 0, \end{aligned} \right\} \quad (5)$$

$$u = 0, \quad T \rightarrow T_\infty, \quad C \rightarrow C_\infty, \quad \text{at } y \rightarrow \infty \quad (6)$$

Where u and v are the velocity components in x – and y – directions respectively. Then u_w is velocity at the wall, v_w represents the velocity of suction/injection, σ is the fluid conductivity, B_0 for magnetic field strength, T for temperature, c_p is the specific heat at constant pressure, $\nu = \frac{\mu}{\rho}$ is the kinematic viscosity, ρ is the fluid density, μ is the coefficient of fluid viscosity, A_0 denotes the rate of stretching surface, $\rho_p c_p$ for heat capacity of nanoparticles, ρc for heat capacity of nanofluid, n is power law index, Γ is positive time constant, D_B is Brownian diffusion coefficient, D_T is Thermophoresis diffusion coefficient, k is thermal conductivity, α is thermal diffusivity.

2.2 Dimensionless analysis

We introduce the following dimensionless variables:

$$\left. \begin{aligned} u = U_0 e^{\frac{x}{2l}} f'(\eta), \quad v = -\sqrt{\frac{U_0 \nu}{2l}} e^{\frac{x}{2l}} (f(\eta) + \eta f'(\eta)), \\ \eta = \sqrt{\frac{U_0}{2\nu l}} y e^{\frac{x}{2l}}, \quad PHF \text{ CASE: } T = T_\infty + \frac{(T_w - T_\infty)}{k} e^{\frac{x}{2l}} \sqrt{\frac{2\nu l}{U_0}} \theta(\eta), \\ PMF \text{ CASE: } C = C_\infty + \frac{(C_w - C_\infty)}{D_B} e^{\frac{x}{2l}} \sqrt{\frac{2\nu l}{U_0}} g(\eta), \end{aligned} \right\} \quad (7)$$

The viscosity will change with temperature as $\mu = \mu_0 e^{-\beta_1 \theta(\eta)}$, where μ_0 is the coefficient of viscosity at the temperature T_w and β_1 is variable viscosity parameter. In general $\beta_1 > 0$ for liquids, $\beta_1 < 0$ for gases and $\beta_1 = 0$ for constant viscosity.

The governing equation reduces to

$$[(1-n) + nWe f''] f''' + [\frac{1}{2} n f'' - (1-n)v^2] \beta_1 \theta' f'' + e^{\beta_1 \theta} [f f'' - 2(f')^2 - M f'] = 0, \quad (8)$$

$$\theta'' + Pr(f \theta' - f' \theta + Nb \ g' \theta' + Nt \ \theta'^2) = 0, \quad (9)$$

$$g'' + Sc(fg' - f'g) + \frac{Nt}{Sc Nb} \theta'' = 0, \quad (10)$$

The transformed boundary conditions are then given by:

$$\left. \begin{aligned} f(0) = -S, \quad f'(0) = 1, \quad \theta'(0) = -1, \quad g'(\eta = 0) = -1, \\ f'(\infty) \rightarrow 0, \quad \theta(\infty) \rightarrow 0, \quad g(\infty) \rightarrow 0. \end{aligned} \right\} \quad (11)$$

$$\left. \begin{aligned} \text{Where, } We = \Gamma \sqrt{\frac{U_0^3 e^{\frac{3x}{l}}}{\nu l}}, \quad M = \frac{2l\sigma B^2}{\rho U_0}, \quad S = V_0 \sqrt{\frac{2l}{\nu U_0}}, \quad Sc = \frac{\nu}{D_B}, \\ Nb = \frac{\rho_b c_b}{\rho c} \frac{C_w - C_\infty}{\nu} D_B, \quad Nt = \frac{\rho_b c_b}{\rho c} \frac{D_T(T_w - T_\infty)}{k T_\infty} e^{\frac{x}{2l}} \sqrt{\frac{2l}{\nu U_0}}, \quad Pr = \frac{\nu}{\alpha}, \end{aligned} \right\} \quad (12)$$

The physical quantities of interest are the skin friction coefficient C_{f_x} , Nusselt number N_{u_x} and Sherwood number Sh_{u_x} are defined as:

$$C_{f_x} = \left(\frac{\tau_w}{\rho U_w^2} \right)_{y=0}, \quad (13)$$

$$N_{u_x} = \left(\frac{x q_w}{k(T_w - T_\infty)} \right)_{y=0}, \quad (14)$$

$$Sh_{u_x} = \left(\frac{x j_w}{D_B(C_w - C_\infty)} \right)_{y=0}, \quad (15)$$

Where, τ_w denotes the shear stress, q_w stands for the heat flux, and j_w represent mass flux and these quantities are defined as [51], [52]:

$$\tau_w = (1 - n)u_y + \frac{n\Gamma}{\sqrt{2}}(u_y)^2, \quad (16)$$

$$q_w = -k \left(\frac{\partial T}{\partial y} \right)_{y=0}, \quad (17)$$

$$j_w = -D_B \left(\frac{\partial C}{\partial y} \right)_{y=0}, \quad (18)$$

Dimensionless forms of C_{f_x} , N_{u_x} and Sh_{u_x} are:

$$-C_{f_x} \sqrt{Re_x} = ((1 - n)f''(0) + \frac{n}{2} We f''^2(0)), \quad (19)$$

$$PHF: \frac{N_{u_x}}{\sqrt{Re_x}} = \frac{1}{\theta(0)}, \quad (20)$$

$$PMF: \frac{Sh_{u_x}}{\sqrt{Re_x}} = \frac{1}{g(0)}, \quad (21)$$

Where, $Re_x = \frac{U_w l}{\nu}$ is the local Reynold number.

2.3 Numerical method for solution

The domain of the system of governing Eqs. (8) to (11) is $0 \leq \eta \leq \eta_\infty$, where η_∞ represents the limit of computation that user has specified. The algebraic mapping can be used [53]:

$$\chi = 2 \frac{\eta}{\eta_\infty} - 1, \quad (22)$$

A mapping from the unbounded region $[0, \infty)$ to restricted domain $[1, -1]$, and we can transform the problem stated by equations Eqs. (8) to (11) for the system:

$$[(1-n) + nWe f''(\chi)] f'''(\chi) + [\frac{1}{2} n f''(\chi) - (1-n)v^2] \beta_1 \theta'(\chi) f''(\chi) + e^{\beta_1 \theta(\chi)} [f(\chi) f''(\chi) - 2(f'(\chi))^2 - M f'(\chi)] = 0, \quad (23)$$

$$\theta''(\chi) + Pr(f(\chi) \theta'(\chi) - f'(\chi) \theta(\chi) + Nb g'(\chi) \theta'(\chi) + Nt \theta'^2(\chi)) = 0, \quad (24)$$

$$g''(\chi) + Sc(f(\chi) g'(\chi) - f'(\chi) g(\chi)) + \frac{Nt}{Sc Nb} \theta''(\chi) = 0, \quad (25)$$

The following gives transformed boundary conditions:

$$\left. \begin{aligned} f(\chi = -1) = -S, \quad f'(\chi = -1) = 1, \quad \theta'(\chi = -1) = -1, \quad g'(\chi = -1) = -1 \\ f'(\chi = 1) = 0, \quad \theta(\chi = 1) = 0, \quad g(\chi = 1) = 0, \end{aligned} \right\} \quad (26)$$

Our method works by starts with a Chebyshev approaching for largest derivatives, f''' , h'' and θ'' . From there, we generate approximate the smaller order derivatives f'' , f' , f , h' , h , θ' and θ , in the following ways:

If we assume that $f''' = \phi(\chi)$, $h'' = \psi(\chi)$ and $\theta'' = \zeta(\chi)$, then the following may be obtained using integration:

$$f''(\chi) = \int_{-1}^{\chi} \phi(\chi) d\chi + C_1^f, \quad (27)$$

$$f'(\chi) = \int_{-1}^{\chi} \int_{-1}^{\chi} \phi(\chi) d\chi d\chi + C_1^f(\chi + 1) + C_2^f, \quad (28)$$

$$f(\chi) = \int_{-1}^{\chi} \int_{-1}^{\chi} \int_{-1}^{\chi} \phi(\chi) d\chi d\chi d\chi + C_1^f \frac{(\chi+1)^2}{2} + C_2^f(\chi + 1) + C_3^f, \quad (29)$$

$$\theta'(\chi) = \int_{-1}^{\chi} \zeta(\chi) d\chi + C_1^\theta, \quad (30)$$

$$\theta(\chi) = \int_{-1}^{\chi} \int_{-1}^{\chi} \zeta(\chi) d\chi d\chi + C_1^\theta(\chi + 1) + C_2^\theta, \quad (31)$$

$$g'(\chi) = \int_{-1}^{\chi} \psi(\chi) d\chi + C_1^g, \quad (32)$$

$$g(\chi) = \int_{-1}^{\chi} \int_{-1}^{\chi} \psi(\chi) d\chi d\chi + C_1^g(\chi + 1) + C_2^g, \quad (33)$$

Using a boundary condition (26), we get:

$$C_1^f = -\frac{1}{2} \int_{-1}^1 \int_{-1}^{\chi} \phi(\chi) d\chi d\chi - \frac{\eta_\infty}{4}, \quad C_2^f = \frac{\eta_\infty}{2}, \quad C_3^f = -S, \quad (34)$$

$$C_1^\theta = -\frac{\eta_\infty}{2}, \quad C_2^\theta = \eta_\infty - \int_{-1}^1 \int_{-1}^\chi \zeta(\chi) d\chi d\chi, \quad (35)$$

$$C_1^g = -\frac{1}{2} - \frac{1}{2} \int_{-1}^1 \int_{-1}^\chi \psi(\chi) d\chi d\chi, \quad C_2^g = 1. \quad (36)$$

As a result, the following are approximations for Eqs. (27) to (33) as follows:

$$f_i(\chi) = \sum_{j=0}^n l_{ij}^f \phi_j + d_i^f, \quad f_i'(\chi) = \sum_{j=0}^n l_{ij}^{f1} \phi_j + d_i^{f1}, \quad f_i''(\chi) = \sum_{j=0}^n l_{ij}^{f2} \phi_j + d_i^{f2}, \quad (37)$$

$$\theta_i(\chi) = \sum_{j=0}^n l_{ij}^\theta \zeta_j + d_i^\theta, \quad \theta_i'(\chi) = \sum_{j=0}^n l_{ij}^{\theta1} \zeta_j + d_i^{\theta1}, \quad (38)$$

$$g_i(\chi) = \sum_{j=0}^n l_{ij}^g \psi_j + d_i^g, \quad g_i'(\chi) = \sum_{j=0}^n l_{ij}^{g1} \psi_j + d_i^{g1}, \quad (39)$$

for all $i = 0(1)n$, where

$$l_{ij}^f = b_{ij}^3 - \frac{(\chi_i+1)^2}{4} b_{nj}^2, \quad d_i^f = -\frac{(\chi_i+1)^2}{8} \eta_\infty + \frac{(\chi_i+1)}{2} \eta_\infty - S, \quad (40)$$

$$l_{ij}^{f1} = b_{ij}^2 - \frac{(\chi_i+1)}{2} b_{nj}^2, \quad d_i^{f1} = -\frac{(\chi_i+1)}{4} \eta_\infty + \frac{\eta_\infty}{2}, \quad (41)$$

$$l_{ij}^{f2} = b_{ij} - \frac{1}{2} b_{nj}^2, \quad d_i^{f2} = -\frac{\eta_\infty}{4}, \quad (42)$$

$$l_{ij}^\theta = b_{ij}^2 - b_{nj}^2, \quad d_i^\theta = \eta_\infty - \frac{(\chi_i+1)}{2} \eta_\infty, \quad (43)$$

$$l_{ij}^{\theta1} = b_{ij}^2, \quad d_i^{\theta1} = -\frac{\eta_\infty}{2}, \quad (44)$$

$$l_{ij}^g = b_{ij}^2 - \frac{(\chi_i+1)}{2} b_{nj}^2, \quad d_i^g = -\frac{(\chi_i+1)}{2} + 1, \quad (45)$$

$$l_{ij}^{g1} = b_{ij}^2 - \frac{1}{2} b_{nj}^2, \quad d_i^{g1} = -\frac{1}{2}, \quad (46)$$

where $\chi_i = -\cos(\frac{i\pi}{n})$ are the Chebyshev points.

$$b_{ij}^2 = (\chi_i - \chi_j) b_{ij},$$

b_{ij} are the elements of the matrix B , as stated in [54]. Eqs. (8) to (11) for the corresponding system of nonlinear equations in the largest derivatives can be transformed into the following Chebyshev spectral by utilizing Eqs. (37) to (46):

$$[(1-n) + nWe(\sum_{j=0}^n l_{ij}^{f2} \phi_j + d_i^{f2})] \phi_i + [\frac{1}{2} n(\sum_{j=0}^n l_{ij}^{f2} \phi_j + d_i^{f2}) - (1-n)v^2] \beta_1 (\sum_{j=0}^n l_{ij}^{\theta1} \zeta_j + d_i^{\theta1}) (\sum_{j=0}^n l_{ij}^{f2} \phi_j + d_i^{f2}) + e^{\beta_1 (\sum_{j=0}^n l_{ij}^{\theta1} \zeta_j + d_i^{\theta1})} [(\sum_{j=0}^n l_{ij}^f \phi_j + d_i^f) (\sum_{j=0}^n l_{ij}^{f2} \phi_j + d_i^{f2}) - 2(\sum_{j=0}^n l_{ij}^{f1} \phi_j + d_i^{f1})^2 - M(\sum_{j=0}^n l_{ij}^{f1} \phi_j + d_i^{f1})] = 0, \quad (47)$$

$$(\sum_{j=0}^n l_{ij}^{\theta2} \zeta_j + d_i^{\theta2}) + \text{Pr}((\sum_{j=0}^n l_{ij}^f \phi_j + d_i^f) (\sum_{j=0}^n l_{ij}^{\theta1} \zeta_j + d_i^{\theta1}) - (\sum_{j=0}^n l_{ij}^{f1} \phi_j + d_i^{f1}) (\sum_{j=0}^n l_{ij}^\theta \zeta_j + d_i^\theta) + Nb(\sum_{j=0}^n l_{ij}^{g1} \psi_j + d_i^{g1}) (\sum_{j=0}^n l_{ij}^{\theta1} \zeta_j + d_i^{\theta1}) + Nt(\sum_{j=0}^n l_{ij}^{\theta1} \zeta_j + d_i^{\theta1})^2) = 0, \quad (48)$$

$$(\sum_{j=0}^n l_{ij}^{g2} \psi_j + d_i^{g2}) + Sc((\sum_{j=0}^n l_{ij}^f \phi_j + d_i^f) (\sum_{j=0}^n l_{ij}^{g1} \psi_j + d_i^{g1}) - (\sum_{j=0}^n l_{ij}^{f1} \phi_j + d_i^{f1}) (\sum_{j=0}^n l_{ij}^g \psi_j + d_i^g)) + \frac{Nt}{Sc Nb} (\sum_{j=0}^n l_{ij}^{\theta1} \zeta_j + d_i^{\theta1})^2 = 0. \quad (49)$$

The computer program was run in MATHEMATICA to ensure accuracy and stability of the results on a PC, and by using Newton's iteration approach with $n = 12$, this system is solved.

3. Results and discussion

To validate the accuracy of the methodology, in Table 1 we compare the present results with the previous one that obtained by Akbar et al., [51] and Amjad et al., [11] considering $We = n = S = \beta_1 = 0$ for different values of M . These studies were selected because they investigate the same type of boundary layer flow and employ similar simplifying assumptions, allowing for a consistent and meaningful comparison. Akbar's study examines the effects of a magnetic field on Eyring–Powell fluid flow over a linearly stretching sheet, while Amjad explores tangent hyperbolic nanofluid flow over an exponentially stretched sheet with prescribed exponential-order surface temperature (PEST) and heat flux (PEHF) conditions. However, both studies do not account for temperature-dependent viscosity, which limits their applicability in systems with significant thermal variation. Furthermore, Akbar assumes fixed thermal and concentration boundary conditions, while Amjad does not consider the combined effects of prescribed heat flux (PHF) and mass flux (PMF) boundary conditions. Our study improves upon these limitations by introducing an exponentially stretching sheet with temperature-dependent viscosity, along with PHF and PMF boundary conditions. This approach provides valuable insights for applications such as polymer extrusion and high-temperature cooling systems. Our results demonstrate a strong agreement with those of previous studies, validating the accuracy and robustness of our approach.

Table 1. Results comparison of $f''(0)$ for various values of M when $We = n = S = \beta_1 = 0$

M	Akbar et al. [51]	Amjad et al. [11]	Present study
0.0	-1.00000	-1.00000	-0.96604
0.5	-1.11803	-1.11803	-1.10997
1.0	-1.41421	-1.41421	-1.41341
5.0	-2.449449	-2.449489	-2.49567
10	-3.31663	-3.316624	-3.40825
100	-10.0498	-10.04987	-10.05985
500	-22.38303	-22.38303	-23.59678
1000	-31.63859	-31.63858	-31.67193

Tables 2-3 shows the impacts on $\frac{Nu_x}{\sqrt{Re_x}}$, $\frac{Sh_x}{\sqrt{Re_x}}$ for several physical parameters. As Weissenberg number We rises the value of the local Nusslet and Sherwood numbers are reduced. Due to the Lorentz effect, that causes fluid motion to slow, by raising the Magnetic field parameter M , the local Nusslet and Sherwood numbers are reduced. As Power law index n enhances the Nusslet number and Sherwood number are decreased. The local Nusslet number and Sherwood number are reduced when the Suction and injection parameter S increases because the stretched surface causes resistivity on fluid flow. When the variable viscosity parameter β_1 goes up, it indicated that Nu_x and Sh_x increase their values. The local Nusslet number is enhanced as Pr raises, but Sh_x falls in its values. The local Sherwood number (Sh_x) rises while Nu_x decreases as Brownian motion Nb grows. Upon increasing Nt , the Nusslet and Sherwood numbers had fallen in their values. Sherwood and Nusslet local numbers are also an increasing function in Sc .

Table 2. Values of $\frac{Nu_x}{\sqrt{Re_x}}$ for different values of $We, n, S, M, \beta_1, Pr, Nb, Nt$, and Sc

We	S	n	M	β_1	Pr	Nb	Nt	Sc	$\frac{Nu_x}{\sqrt{Re_x}}$
0.0	0.2	0.3	0.2	0.1	0.5	0.5	0.5	1.0	0.34028
0.3	0.2	0.3	0.2	0.1	0.5	0.5	0.5	1.0	0.33192
0.5	0.2	0.3	0.2	0.1	0.5	0.5	0.5	1.0	0.32538
0.3	0.0	0.3	0.2	0.1	0.5	0.5	0.5	1.0	0.35329
0.3	0.2	0.3	0.2	0.1	0.5	0.5	0.5	1.0	0.33192
0.3	0.3	0.3	0.2	0.1	0.5	0.5	0.5	1.0	0.32362
0.3	0.2	0.0	0.2	0.1	0.5	0.5	0.5	1.0	0.38112
0.3	0.2	0.2	0.2	0.1	0.5	0.5	0.5	1.0	0.35128
0.3	0.2	0.3	0.2	0.1	0.5	0.5	0.5	1.0	0.33192
0.3	0.2	0.3	0.0	0.1	0.5	0.5	0.5	1.0	0.36589
0.3	0.2	0.3	0.2	0.1	0.5	0.5	0.5	1.0	0.33192
0.3	0.2	0.3	0.3	0.1	0.5	0.5	0.5	1.0	0.31813
0.3	0.2	0.3	0.2	0.0	0.5	0.5	0.5	1.0	0.36227
0.3	0.2	0.3	0.2	0.2	0.5	0.5	0.5	1.0	0.29366
0.3	0.2	0.3	0.2	0.3	0.5	0.5	0.5	1.0	0.23971
0.3	0.2	0.3	0.2	0.3	0.1	0.5	0.5	1.0	0.16025
0.3	0.2	0.3	0.2	0.3	0.2	0.5	0.5	1.0	0.20467
0.3	0.2	0.3	0.2	0.3	0.3	0.5	0.5	1.0	0.25001
0.3	0.2	0.3	0.2	0.3	0.5	0.1	0.5	1.0	0.37319
0.3	0.2	0.3	0.2	0.3	0.5	0.2	0.5	1.0	0.36236
0.3	0.2	0.3	0.2	0.3	0.5	0.3	0.5	1.0	0.35188
0.3	0.2	0.3	0.2	0.3	0.5	0.5	0.0	1.0	0.41241
0.3	0.2	0.3	0.2	0.3	0.5	0.5	0.3	1.0	0.36303
0.3	0.2	0.3	0.2	0.3	0.5	0.5	0.5	1.0	0.33192
0.3	0.2	0.3	0.2	0.3	0.5	0.5	0.5	0.1	0.15995
0.3	0.2	0.3	0.2	0.3	0.5	0.5	0.5	0.3	0.25538
0.3	0.2	0.3	0.2	0.3	0.5	0.5	0.5	0.5	0.30018

In this section, we conduct a numerical investigation using the Chebyshev spectral method to analyze the flow of tangent hyperbolic nanofluid (a non-Newtonian fluid) over an exponentially stretching surface, incorporating the combined effects of variable viscosity, magnetic field, and PHF/PMF boundary conditions. For velocity, temperature, and concentration profiles, the impacts of physical parameters has been investigated for the variable viscosity β_1 , power law index n , magnetic parameter M , suction/injection parameter S , Brownian motion parameter Nb , thermophoretic parameter Nt , and Schmidt number Sc . The system of ODEs obtained in the Eqs (8) to (11) are solved using Chebyshev Spectral Method to find the numerical solutions for transformed differential system.

The ranges of all physical variables used in this study are [55]:

$$O(\beta_1) \sim 0 \rightarrow 0.4, \quad O(n) \sim 0.1 \rightarrow 0.5, \quad O(M) \sim 0.1 \rightarrow 0.5, \quad O(S) \sim -0.4 \rightarrow 0.4, \\ O(We) \sim 0 \rightarrow 0.5, \quad O(Nt) \sim 0 \rightarrow 0.6, \quad O(Nb) \sim 0.1 \rightarrow 1, \quad O(Pr) \sim 0.1 \rightarrow 2, \\ O(Sc) \sim 0.1 \rightarrow 1.6.$$

Table 3. Values of $\frac{Sh_x}{\sqrt{Re_x}}$ for different values of $We, n, S, M, \beta_1, Pr, Nb, Nt$, and Sc

We	S	n	M	β_1	Pr	Nb	Nt	Sc	$\frac{Sh_x}{\sqrt{Re_x}}$
0.0	0.2	0.3	0.2	0.1	0.5	0.5	0.5	1.0	0.49560
0.3	0.2	0.3	0.2	0.1	0.5	0.5	0.5	1.0	0.48707
0.5	0.2	0.3	0.2	0.1	0.5	0.5	0.5	1.0	0.48049
0.3	0.0	0.3	0.2	0.1	0.5	0.5	0.5	1.0	0.52138
0.3	0.2	0.3	0.2	0.1	0.5	0.5	0.5	1.0	0.48707
0.3	0.3	0.3	0.2	0.1	0.5	0.5	0.5	1.0	0.47148
0.3	0.2	0.0	0.2	0.1	0.5	0.5	0.5	1.0	0.54066
0.3	0.2	0.2	0.2	0.1	0.5	0.5	0.5	1.0	0.50750
0.3	0.2	0.3	0.2	0.1	0.5	0.5	0.5	1.0	0.48707
0.3	0.2	0.3	0.0	0.1	0.5	0.5	0.5	1.0	0.52228
0.3	0.2	0.3	0.2	0.1	0.5	0.5	0.5	1.0	0.48707
0.3	0.2	0.3	0.3	0.1	0.5	0.5	0.5	1.0	0.47321
0.3	0.2	0.3	0.2	0.0	0.5	0.5	0.5	1.0	0.51932
0.3	0.2	0.3	0.2	0.2	0.5	0.5	0.5	1.0	0.44906
0.3	0.2	0.3	0.2	0.3	0.5	0.5	0.5	1.0	0.40138
0.3	0.2	0.3	0.2	0.3	0.1	0.5	0.5	1.0	0.57247
0.3	0.2	0.3	0.2	0.3	0.2	0.5	0.5	1.0	0.53017
0.3	0.2	0.3	0.2	0.3	0.3	0.5	0.5	1.0	0.57077
0.3	0.2	0.3	0.2	0.3	0.5	0.1	0.5	1.0	0.20041
0.3	0.2	0.3	0.2	0.3	0.5	0.2	0.5	1.0	0.31734
0.3	0.2	0.3	0.2	0.3	0.5	0.3	0.5	1.0	0.39375
0.3	0.2	0.3	0.2	0.3	0.5	0.5	0.0	1.0	0.74695
0.3	0.2	0.3	0.2	0.3	0.5	0.5	0.3	1.0	0.56122
0.3	0.2	0.3	0.2	0.3	0.5	0.5	0.5	1.0	0.48707
0.3	0.2	0.3	0.2	0.3	0.5	0.5	0.5	0.1	0.05984
0.3	0.2	0.3	0.2	0.3	0.5	0.5	0.5	0.3	0.12701
0.3	0.2	0.3	0.2	0.3	0.5	0.5	0.5	0.5	0.22330

3.1 Velocity distribution

Figure 3 (a-d) displays the impact of velocity profile versus η which is dependent on β_1, M, S , and n . The effects of β_1 on the velocity $f'(\eta)$ are depicted in Figure 3(a). As β_1 increases, the boundary-layer thickness diminishes and the overall velocity profile decreases a result of larger temperature gradients between the surface and the ambient fluid. Moreover, for $\beta_1 > 0$ the velocity near the wall flattens more rapidly than in the Newtonian case ($\beta_1 = 0$), indicating that the non-Newtonian tangent hyperbolic behavior further reduces flow resistance. The effect of power law index n on $f'(\eta)$ is shown graphically in Figure 3(b). It is obvious that when n grows, the velocity profile falls. From a physical standpoint, its influence on the fluid's rheological characteristics is what is responsible for the drop in velocity distribution linked to a raised power law index parameter. Physically, the fluid's reaction to shear stresses is primarily responsible for the decrease in nanofluid velocity linked to the power law index. Fluid velocity decreases when the power law index rises, indicating increased resistance to shear. It is depicted in Figure 3(c) that a reduction in the velocity profile as the value of the magnetic parameter M rises according to the retarding force causes. In a physical sense, as the magnetic parameter rises, so does the Lorentz force applied to the fluid. As a result, the fluid moves more slowly as a result of the decreased fluid velocity. The effect of the Suction and injection parameter S is depicted in Figure 3(d), where the

velocity profile grows with increasing for injection/suction parameter. Physically, while the velocity profile grows with increased suction, it reduces with increased injection. The reason for this is that when the fluid is injected into the system close to the surface, it takes up space next to the wall, increasing the momentum boundary thickness. In a suction case the fluid in the surrounding area of the surface moves out, which complicates the formation of the boundary layer. Consequently, the immediate effects of the injection and suction is that they change and decrease the boundary layer thickness for the velocity profile.

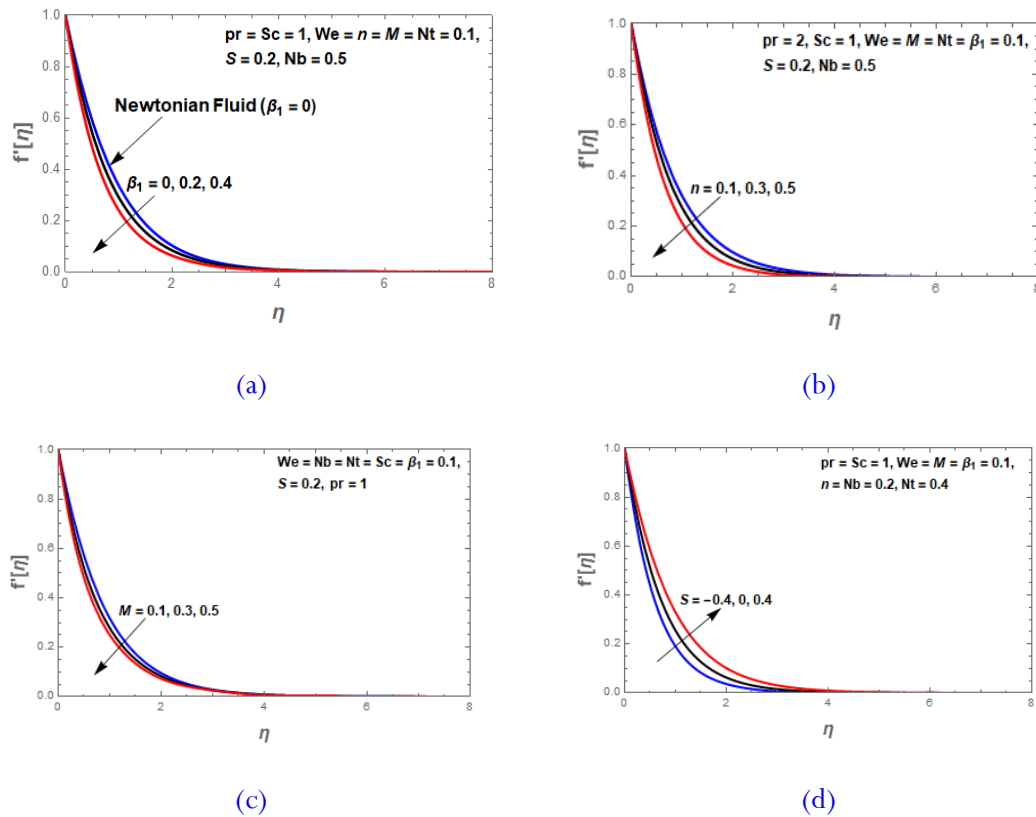


Figure 3. Velocity profiles $f'(\eta)$ versus η for various values of (a) β_1 (b) n (c) M (d) S

3.2 Temperature distribution

The influence of β_1 on temperature verses η is shown in Figure 4(a). It has been noticed that an rises in the fluid viscosity parameter β_1 tends to in an increase in the thermal boundary layer thickness. As a result, $\theta(\eta)$ values rise. Consequently, a rise in β_1 raises the fluid temperature. The temperature variation for a power law index n is displayed in Figure 4(b), where the temperature is increased. Physically, a rise in n causes a rise in viscosity. As a result of a surge in viscosity, the fluid temperature rises. Figures 4(c) - 4(d) presents the impact of magnetic parameter M and Suction/Injection parameter S on $\theta(\eta)$. These figures conclude that temperature grow for larger values of M, S . Physically, the idea is that when the magnetic parameter increases, Lorentz force is created and friction is created on the flow. Friction increases the amount of heat energy produced, which in turn raises the temperature profile in the flow. Figures 4(e) - 4(f) are depicted to interpret the temperature ($\theta(\eta)$) profile for different values of Nt, Nb . The Figures 4(e) - 4(f) display the variation of Nt and Nb for ($\theta(\eta)$). Both the temperature and corresponding layer thickness exhibit similar behavior. For larger Nt , fluid particles rise from the system's hot to cold regions. It results from a rise in the thermophoresis force, which raises the temperature profile (refer to Figure 4(e)). As Nb is estimated higher, the temperature rises due to enhanced random motion of the liquid particles.

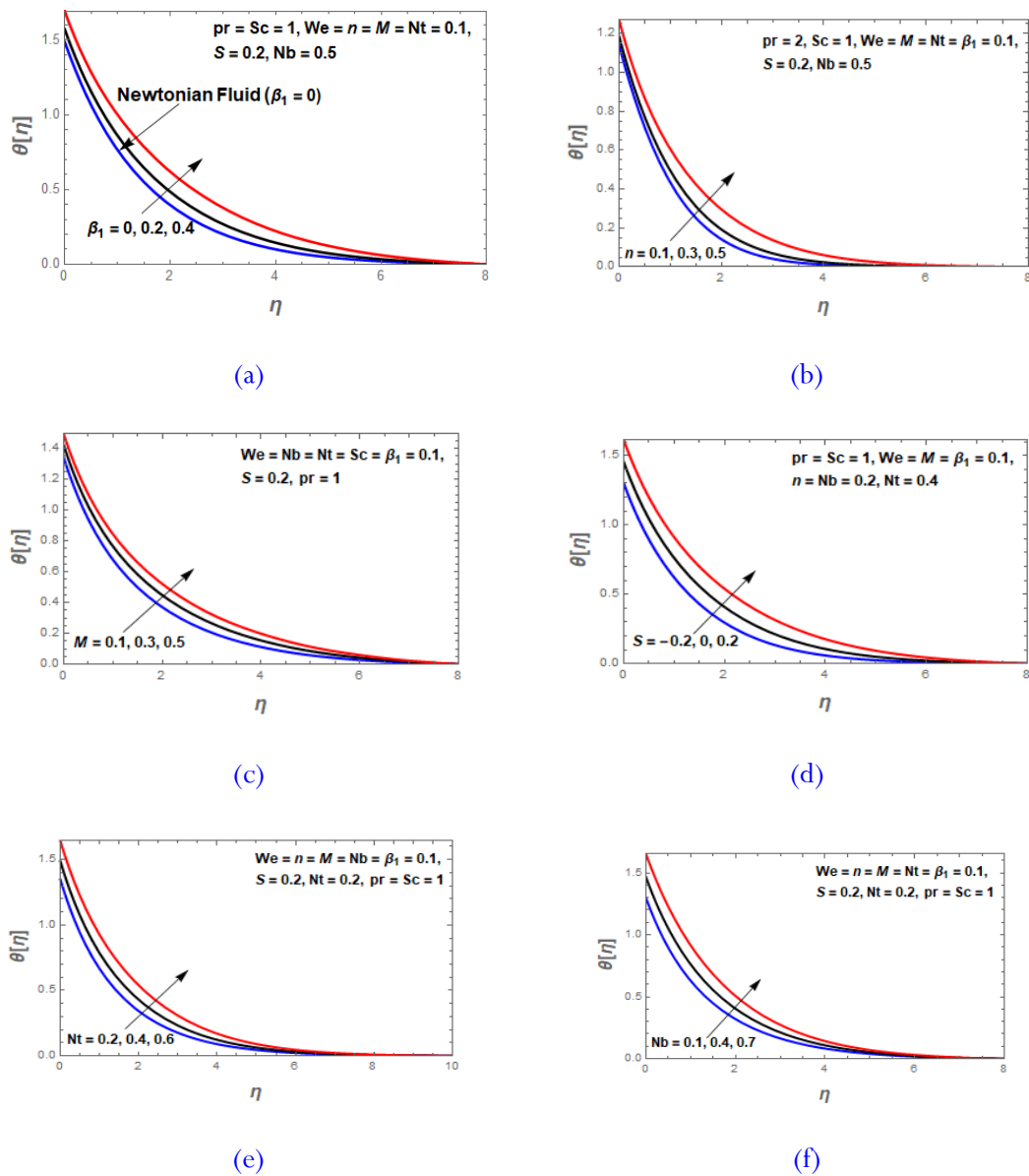


Figure 4. Temperature profiles ($\theta(\eta)$) versus η for different values of (a) β_1 (b) n (c) M (d) S (e) Nt (f) Nb

3.3 Concentration distribution

The impact of β_1 , n , S , and Nt on $g(\eta)$ is depicted in Figure 5(a-d), concentration profiles grow for larger values of β_1 , n , S and additionally, an raise in the thermophoretic parameters Nt was shown to enhance the concentration levels. As a result of the nanoparticles resistance to the heated surface during the thermophoresis process, they scatter from the warm surface into the surrounding fluid. In this manner the thermophoretic force is responsible for the transfer of heat from the surface to the flowing fluid through nanoparticles. The concentration boundary layer gets thicker. The behavior of Nb on $g(\eta)$ is depicted in Figure 5(e). A reduction in the concentration of nanofluid results from raising Nb due to Brownian motion pushes the particles outside of the fluid system as the boundary layer warms. As a result, as particle size decreases, nanoparticle mobility increases and thermal conduction is improved as Nb increases. The main component of a nanofluid is a two-phase system where the kinetic energy is increased by the arbitrary motion of the nanoparticles. However, Brownian motion has a significant impact on the diffusion of nanoparticles. When Brownian motion is present, the concentration boundary layer's thickness decreases. Figure 5(f)

shows that the variation of Sc on $g(\eta)$. There is a diminishing effect as Sc 's value increases. As Sc rises, the concentration boundary layer thickness reduces because of a decrease in mass diffusivity.

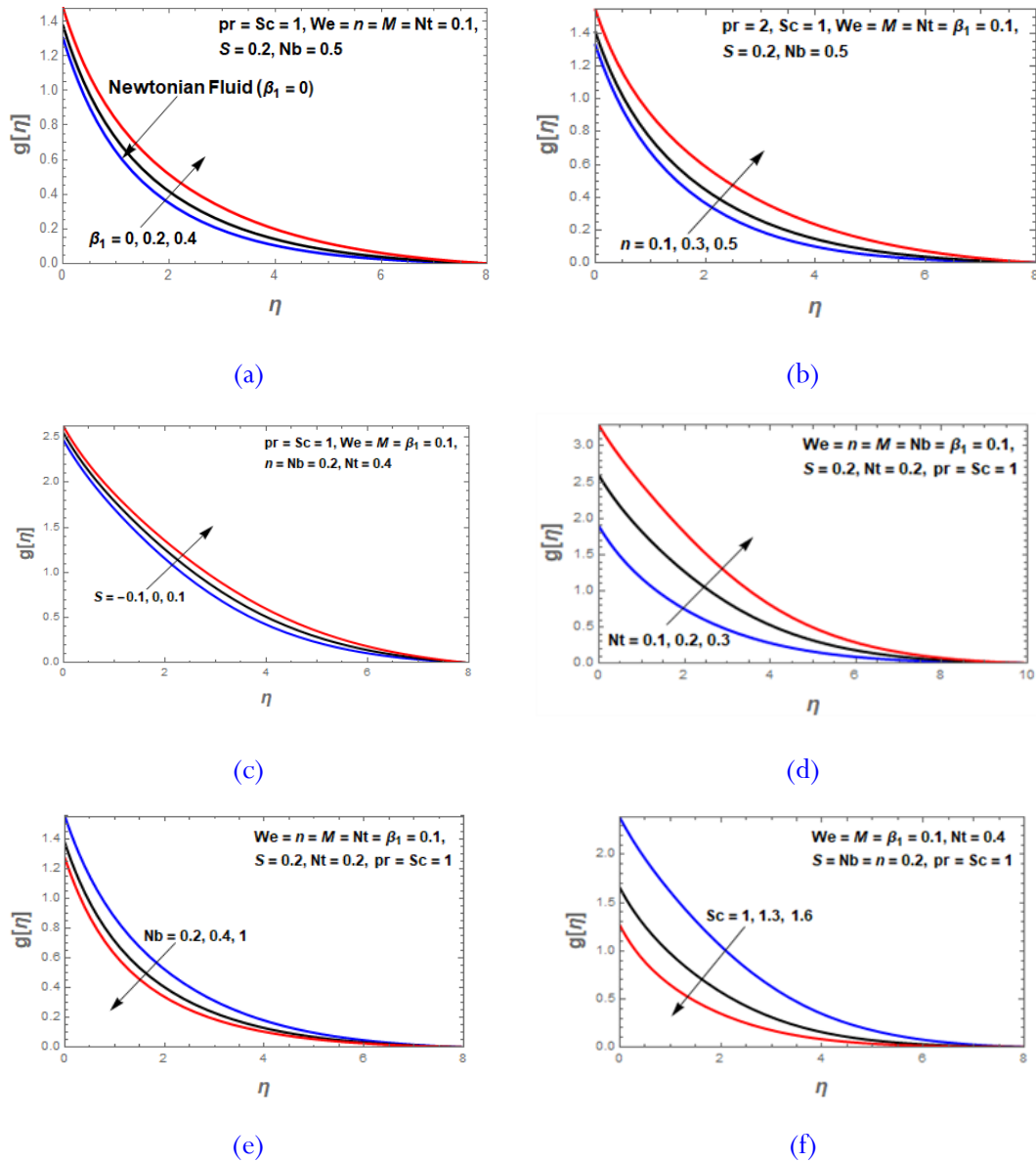


Figure 5. Concentration profiles ($g(\eta)$) versus η for various values of (a) β_1 (b) n (c) S (d) Nt and (e) Nb (f) Sc

3.4 Skin friction distribution

Figure 6(a) demonstrates the increase in the skin friction coefficient with higher Weissenberg numbers (We). As We grows, the fluid's elasticity weakens its resistance to shear, which results in reduced skin friction and a thinner boundary layer. In Figure 6(b) shows the impact of different suction and injection parameter values S on the $C_f\sqrt{Re_x}$. It appears that enhancing the suction and injection parameters allows for better control of the flow near the surface, which reduces friction and boosts overall efficiency in various engineering applications. This can result in energy savings, improved performance, and greater system durability. Figure 6(c) illustrates the impact of the power law index n on $C_f\sqrt{Re_x}$. It shows that as n rises, $C_f\sqrt{Re_x}$ reduces. Figures 6(d) and 6(e) depict the impression of the growing magnetic field parameter M and variable viscosity β_1 on $C_f\sqrt{Re_x}$. Figure 6(a) illustrates how the skin friction coefficient rises with stronger magnetic field

parameters. This is due to the magnetic field generating resistive forces (Lorentz forces) in the fluid, which thickens the boundary layer and restricts the flow. In engineering applications, this leads to higher energy consumption or the need for more powerful equipment to overcome the added resistance. Designers must consider these factors when applying magnetic fields for flow control. Figure 6(e) depicts the rise in the skin friction coefficient with an increase in β_1 . Physically, when the viscosity of a fluid increases, it leads to greater resistance to flow near the surface, causing the boundary layer to thicken and the shear stress to increase. This results in a higher skin friction coefficient. In engineering applications, this means higher energy usage, increased wear on equipment, and potentially lower efficiency in systems that depend on fluid flow. Designers must consider variable viscosity in areas such as lubrication, fluid transport, heat exchangers, and aerodynamics to optimize performance and reduce energy costs.

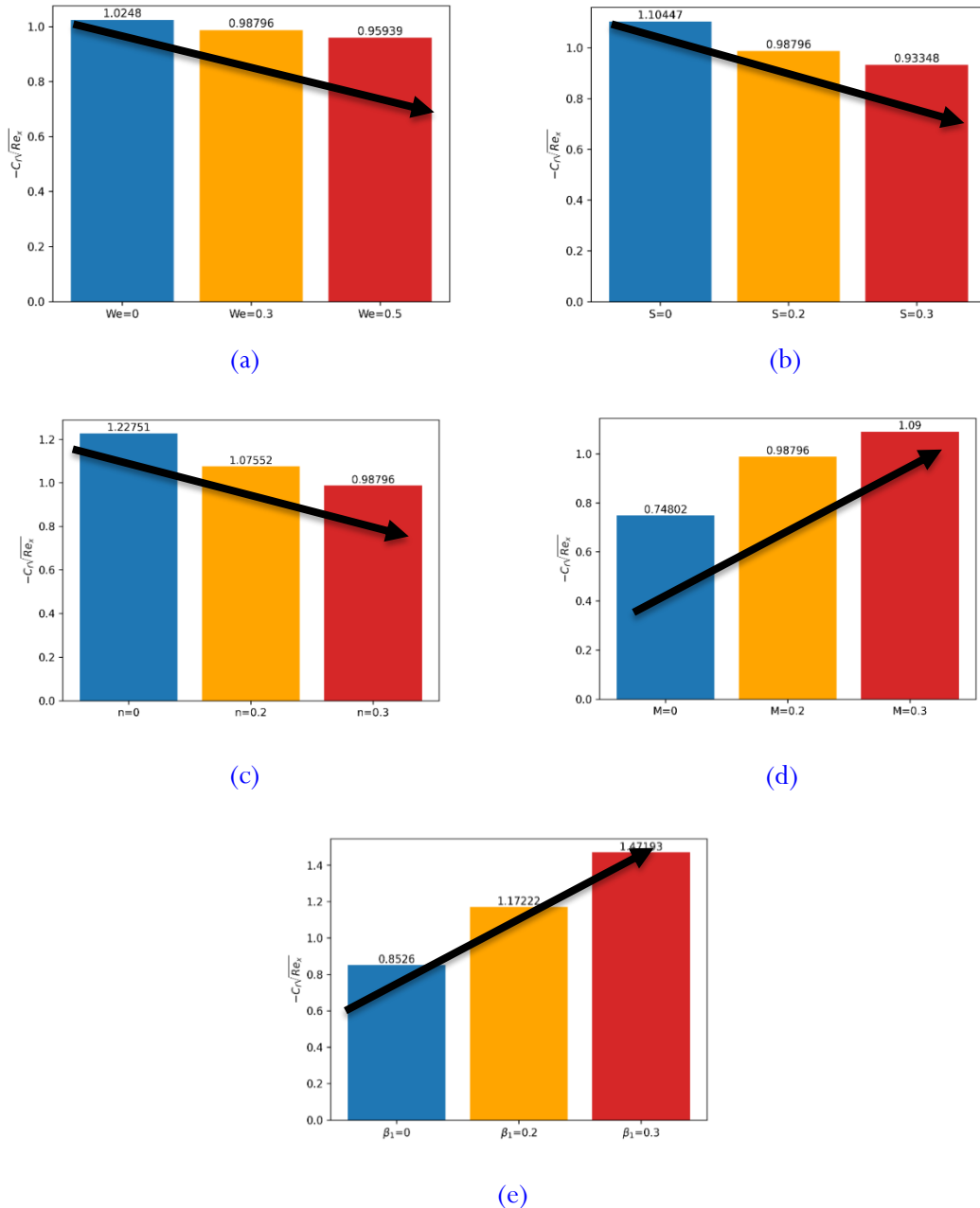


Figure 6. Bar chart representation of skin friction profile $-C_f\sqrt{Re_x}$ for different parameters (a) We (b) S (c) n (d) M (e) β_1 with $Pr = Nb = 0.5$, and $Sc = 1$

3.5 Limitations of current work

Our study acknowledges several limitations that could influence the generalizability and accuracy of the results. The mathematical model employed in our work simplifies real-world complexities, potentially omitting certain critical factors that may influence the behavior of the system. Additionally, the assumptions made regarding the boundary conditions may not encompass all possible physical scenarios, which could limit the applicability of our conclusions. While the Chebyshev Spectral Method has proven to be effective in our analysis, it does have certain limitations, particularly under specific conditions that could affect the accuracy of the results. Moreover, the sensitivity of the results to the selected parameter values in the simulations suggests that variations in these parameters could impact the findings significantly. Finally, our study focuses on particular nanofluids and conditions, which may restrict the broader applicability of the findings to other materials or scenarios. To overcome these limitations, future research could consider more complex models that incorporate a broader range of real-world factors and boundary conditions. It would also be beneficial to test a wider variety of parameters and conditions to improve the robustness of the findings. Exploring alternative numerical methods and studying different nanofluids under diverse conditions would help broaden the scope and applicability of the results, leading to a deeper understanding of the underlying phenomena.

4. Conclusion

In this work analyzed Numerical solution of the variable fluid viscosity on MHD Non-Newtonian nanofluid of variable viscosity with prescribed exponential order heat and mass flux through an exponentially stretching surface. Using the proper similarity transformations, the governing equations of nonlinear PDEs is converted into the system of nonlinear ODEs. The transformed system of modelled equations was solved using Chebyshev spectral method. There was a strong agreement between our findings and those from previously published works. The flow and heat transfer details are highlighted by the numerical results are shown in tabular and graphical. These are the model's most significant outcomes, listed in order of importance.

- The Skin friction coefficient is larger for Newtonian fluid ($n = 0$) than Non-Newtonian ($n \neq 0$).
- The Nusslet and Sherwood numbers are less for nanofluid than clear fluid.
- The rate of change of the velocity, temperature and concentration profiles have a term which directly proportional to viscosity ($\beta_1 \neq 0$) than constant viscosity ($\beta_1 = 0$).
- The velocity and temperature profile $\theta(\eta)$ will rises with the increase of Suction Injection parameter S .
- The rising in the Schmidt number Sc causes an reduces in the concentration profile $g(\eta)$, while enhanced in the case of $\beta_1 \neq 0, n \neq 0, S \neq 0, Nt \neq 0$.
- In the future, the suggested fluid flow model has to be applied to other physical environments. To obtain the maximum heat transfer rate, the application of several nanoparticles from the current study will be considered. As a result, the suggested model should therefore include contributions to the current industrial challenges. For comparison and reference reasons.

Author's declaration

Author contribution

Mohamed Magdy Ghazy, Ahmed Mostafa Megahed and Rabea Elshennawy Abo-Elkhair: Carried out the formal analysis, investigation, conceptualization and drafted the

manuscript. **Khalid Saad Mekheimer:** Carried out methodology, review, editing and supervision. All authors read and approved the final manuscript.

Funding statement

This research did not receive any specific grant from funding agencies in the public, commercial, or not-for-profit sectors.

Data Availability

All data generated or analyzed during this study are included in this published article.

Acknowledgement

The authors are grateful to the referees for their most valuable comments that improved the paper considerably.

Competing interest

The authors declare that they have no competing interests.

Ethical clearance

This research does not involve humans as subjects.

AI statement

This article is the original work of the author without using AI tools for writing sentences and/or creating/editing tables and figures in this manuscript.

Publisher's and Journal's note

Universitas Negeri Padang as the publisher, and Editor of Teknomekanik state that there is no conflict of interest towards this article publication.

References

- [1] W. Abbas, A. M. Megahed, M. H. Beniamen, and R. Awadalla, "Investigation of Slip Phenomenon of Tangent Hyperbolic Nanofluid Flow Due to a Vertical Sheet With Thermal Radiation," *Journal of Nonlinear Mathematical Physics*, vol. 32, no. 1, p. 13, Mar. 2025, <https://doi.org/10.1007/s44198-025-00266-9>
- [2] I. Pop and D. B. Ingham, *Convective Heat Transfer: Mathematical and Computational Modelling of Viscous Fluids and Porous Media*. Elsevier, 2001. <https://doi.org/10.1016/B978-0-08-043878-8.X5000-7>
- [3] B. C. Sakiadis, "Boundary-layer behavior on continuous solid surfaces: I. Boundary-layer equations for two-dimensional and axisymmetric flow," *AIChE Journal*, vol. 7, no. 1, pp. 26–28, Mar. 1961, <https://doi.org/10.1002/aic.690070108>
- [4] L. J. Crane, "Flow past a stretching plate," *Zeitschrift für angewandte Mathematik und Physik ZAMP*, vol. 21, no. 4, pp. 645–647, Jul. 1970, <https://doi.org/10.1007/BF01587695>
- [5] C. Y. Wang, "Liquid film on an unsteady stretching surface," *Q Appl Math*, vol. 48, no. 4, pp. 601–610, Dec. 1990, <https://doi.org/10.1090/qam/1079908>

- [6] R. Cortell, "A note on magnetohydrodynamic flow of a power-law fluid over a stretching sheet," *Appl Math Comput*, vol. 168, no. 1, pp. 557–566, Sep. 2005, <https://doi.org/10.1016/j.amc.2004.09.046>
- [7] M. Y. Malik, T. Salahuddin, A. Hussain, and S. Bilal, "MHD flow of tangent hyperbolic fluid over a stretching cylinder: Using Keller box method," *J Magn Magn Mater*, vol. 395, pp. 271–276, Dec. 2015, <https://doi.org/10.1016/j.jmmm.2015.07.097>
- [8] M. Amjad, M. N. Khan, K. Ahmed, I. Ahmed, T. Akbar, and S. M. Eldin, "Magnetohydrodynamics tangent hyperbolic nanofluid flow over an exponentially stretching sheet: Numerical investigation," *Case Studies in Thermal Engineering*, vol. 45, p. 102900, May 2023, <https://doi.org/10.1016/j.csite.2023.102900>
- [9] R. Ali, M. R. Khan, A. Abidi, S. Rasheed, and A. M. Galal, "Application of PEST and PEHF in magneto-Williamson nanofluid depending on the suction/injection," *Case Studies in Thermal Engineering*, vol. 27, p. 101329, Oct. 2021, <https://doi.org/10.1016/j.csite.2021.101329>
- [10] M. Khan, A. Hussain, M. Y. Malik, T. Salahuddin, and F. Khan, "Boundary layer flow of MHD tangent hyperbolic nanofluid over a stretching sheet: A numerical investigation," *Results Phys*, vol. 7, pp. 2837–2844, 2017, <https://doi.org/10.1016/j.rinp.2017.07.061>
- [11] K. S. Mekheimer, M. A. Seddeek, R. E. Abo-Elkhair, A. M. Salem, and A. A. Gadelhak, "The Thermal Flow of Maxwell Nanofluid Over a Stretching Sheet with Electro-Kinetic and Viscous Dissipation Effects: A Buongiorno's Model," 2025, pp. 221–252. https://doi.org/10.1007/978-981-96-1570-4_10
- [12] E. Alali and A. M. Megahed, "MHD dissipative Casson nanofluid liquid film flow due to an unsteady stretching sheet with radiation influence and slip velocity phenomenon," *Nanotechnol Rev*, vol. 11, no. 1, pp. 463–472, Jan. 2022, <https://doi.org/10.1515/ntrev-2022-0031>
- [13] R. I. Yahaya, F. M. Ali, N. M. Arifin, N. S. Khashi'ie, and S. S. P. M. Isa, "MHD flow of hybrid nanofluid past a stretching sheet: double stratification and multiple slips effects," *Mathematical Modeling and Computing*, vol. 9, no. 4, pp. 871–881, 2022, <https://doi.org/10.23939/mmc2022.04.871>
- [14] F. Shahzad *et al.*, "Thermal analysis for Al₂O₃–sodium alginate magnetized Jeffrey's nanofluid flow past a stretching sheet embedded in a porous medium," *Sci Rep*, vol. 12, no. 1, p. 3287, Feb. 2022, <https://doi.org/10.1038/s41598-022-06983-1>
- [15] W. Abbas, A. M. Megahed, M. A. Ibrahim, and A. A. M. Said, "Non-Newtonian Slippery Nanofluid Flow Due to a Stretching Sheet Through a Porous Medium with Heat Generation and Thermal Slip," *Journal of Nonlinear Mathematical Physics*, vol. 30, no. 3, pp. 1221–1238, Jun. 2023, <https://doi.org/10.1007/s44198-023-00125-5>
- [16] C. Vittal, V. Tankasala, P. Ashok, S. Renuka, M. Chenna, and K. Reddy, "MHD Boundary Layer Flow and Heat Transfer to Sisko Nanofluid Over a Nonlinear Stretching Sheet," *International Journal of Engineering Research & Technology*, vol. 12, no. 7, Aug. 2023, <https://doi.org/10.17577/IJERTV12IS070138>
- [17] N. S. Akbar, A. Al-Zubaidi, S. Saleem, and S. A. M. Alsallami, "Variable fluid properties analysis for thermally laminated 3-dimensional magnetohydrodynamic non-Newtonian nanofluid over a stretching sheet," *Sci Rep*, vol. 13, no. 1, p. 3231, Feb. 2023, <https://doi.org/10.1038/s41598-023-30233-7>
- [18] H. A. Nabwey, A. M. Rashad, W. A. Khan, S. M. M. El-Kabeir, and S. AbdElnaem, "Heat transfer in MHD flow of Carreau ternary-hybrid nanofluid over a curved surface stretched exponentially," *Front Phys*, vol. 11, Jun. 2023, <https://doi.org/10.3389/fphy.2023.1212715>
- [19] M. Naveed, M. Imran, and S. Gul, "Heat transfer analysis in hydromagnetic flow of couple stress fluid in presence of homogeneous and heterogeneous chemical reactions over a porous oscillatory stretchable sheet," *Advances in Mechanical Engineering*, vol. 15, no. 2, Feb. 2023, <https://doi.org/10.1177/16878132231155823>

- [20] A. M. Amer, S. A. S. Al Rashdi, N. I. Ghoneim, and A. M. Megahed, "Tangent hyperbolic nanofluid flowing over a stretching sheet through a porous medium with the inclusion of magnetohydrodynamic and slip impact," *Results in Engineering*, vol. 19, p. 101370, Sep. 2023, <https://doi.org/10.1016/j.rineng.2023.101370>
- [21] N. S. Yousef, A. M. Megahed, N. I. Ghoneim, M. Elsafi, and E. Fares, "Chemical reaction impact on MHD dissipative Casson-Williamson nanofluid flow over a slippery stretching sheet through porous medium," *Alexandria Engineering Journal*, vol. 61, no. 12, pp. 10161–10170, Dec. 2022, <https://doi.org/10.1016/j.aej.2022.03.032>
- [22] Kh. S. Mekheimer, W. Abbas, M. M. Ghazy, A. M. A. Moawad, and R. E. Abo-Elkhair, "Unsteady squeezing Casson fluid through rotating discs under the variable magnetic field, cross diffusion and chemical reaction effects," *Int J Mod Phys B*, vol. 38, no. 16, Jun. 2024, <https://doi.org/10.1142/S0217979224502011>
- [23] A. A. Gadelhak, Kh. S. Mekheimer, M. A. Seddeek, R. E. Abo-Elkhair, K. K. Ali, and A. M. Salem, "Energy Transport of Williamson Nano-fluid over a Curved Stretching Surface by Means of FDM," *Bionanoscience*, vol. 13, no. 3, pp. 1116–1125, Sep. 2023, <https://doi.org/10.1007/s12668-023-01120-2>
- [24] S. U. S. Choi and J. A. Eastman, "Enhancing thermal conductivity of fluids with nanoparticles," United States, 1995.
- [25] J. Buongiorno, L.-W. Hu, S. J. Kim, R. Hannink, B. Truong, and E. Forrest, "Nanofluids for Enhanced Economics and Safety of Nuclear Reactors: An Evaluation of the Potential Features, Issues, and Research Gaps," *Nucl Technol*, vol. 162, no. 1, pp. 80–91, Apr. 2008, <https://doi.org/10.13182/NT08-A3934>
- [26] X.-Q. Wang and A. S. Mujumdar, "A review on nanofluids - part I: theoretical and numerical investigations," *Brazilian Journal of Chemical Engineering*, vol. 25, no. 4, pp. 613–630, Dec. 2008, <https://doi.org/10.1590/S0104-66322008000400001>
- [27] W. A. Khan and I. Pop, "Boundary-layer flow of a nanofluid past a stretching sheet," *Int J Heat Mass Transf*, vol. 53, no. 11–12, pp. 2477–2483, May 2010, <https://doi.org/10.1016/j.ijheatmasstransfer.2010.01.032>
- [28] T. Hayat, M. Waqas, M. I. Khan, and A. Alsaedi, "Analysis of thixotropic nanomaterial in a doubly stratified medium considering magnetic field effects," *Int J Heat Mass Transf*, vol. 102, pp. 1123–1129, Nov. 2016, <https://doi.org/10.1016/j.ijheatmasstransfer.2016.06.090>
- [29] M. Ferdows, MD. Shamshuddin, S. O. Salawu, and K. Zaimi, "Numerical simulation for the steady nanofluid boundary layer flow over a moving plate with suction and heat generation," *SN Appl Sci*, vol. 3, no. 2, p. 264, Feb. 2021, <https://doi.org/10.1007/s42452-021-04224-0>
- [30] P. S. Reddy and P. Sreedevi, "MHD boundary layer heat and mass transfer flow of nanofluid through porous media over inclined plate with chemical reaction," *Multidiscipline Modeling in Materials and Structures*, vol. 17, no. 2, pp. 317–336, Jul. 2020, <https://doi.org/10.1108/MMMS-03-2020-0044>
- [31] V. B. Awati, A. Goravar, and A. Wakif, "Analysis of unsteady boundary layer flow of nanofluids with heat transfer over a permeable stretching/shrinking sheet via a shifted Chebyshev collocation method," *Waves in Random and Complex Media*, pp. 1–27, Dec. 2022, <https://doi.org/10.1080/17455030.2022.2157515>
- [32] H. Maiti and S. Mukhopadhyay, "Existence of MHD boundary layer hybrid nanofluid flow through a divergent channel with mass suction and injection," *Chemical Engineering Journal Advances*, vol. 14, p. 100475, May 2023, <https://doi.org/10.1016/j.cej.2023.100475>
- [33] A. Shahid, M. M. Bhatti, R. Ellahi, and K. S. Mekheimer, "Numerical experiment to examine activation energy and bi-convection Carreau nanofluid flow on an upper paraboloid porous surface: Application in solar energy," *Sustainable Energy Technologies and Assessments*, vol. 52, p. 102029, Aug. 2022, <https://doi.org/10.1016/J.SETA.2022.102029>

- [34] B. K. Sharma, U. Khanduri, N. K. Mishra, and Kh. S. Mekheimer, "Combined effect of thermophoresis and Brownian motion on MHD mixed convective flow over an inclined stretching surface with radiation and chemical reaction," *Int J Mod Phys B*, vol. 37, no. 10, Apr. 2023, <https://doi.org/10.1142/S0217979223500959>
- [35] B. Jalili, M. Emad, P. Jalili, D. Domiri Ganji, S. Saleem, and E. M. Tag-eldin, "Thermal analysis of boundary layer nanofluid flow over the movable plate with internal heat generation, radiation, and viscous dissipation," *Case Studies in Thermal Engineering*, vol. 49, p. 103203, Sep. 2023, <https://doi.org/10.1016/J.CSITE.2023.103203>
- [36] U. Hayat, R. Ali, S. Shaiq, and A. Shahzad, "A numerical study on thin film flow and heat transfer enhancement for copper nanoparticles dispersed in ethylene glycol," *REVIEWS ON ADVANCED MATERIALS SCIENCE*, vol. 62, no. 1, Jun. 2023, <https://doi.org/10.1515/rams-2022-0320>
- [37] S. A. S. Al Rashdi, N. I. Ghoneim, A. M. Megahed, and A. M. Amer, "Enhancement of heat mass transmission characteristics through a non-Newtonian nanofluid model due to a convectively heated stretched sheet which exposed to a magnetic field," *Results in Engineering*, vol. 18, p. 101180, Jun. 2023, <https://doi.org/10.1016/J.RINENG.2023.101180>
- [38] M. M. Magdy, W. Abbas, Kh. S. Mekheimer, and M. S. Emam, "Ferro-Fluid Flow and Heat Transfer over Unsteady Stretching Sheet in the Presence of a Nonuniform Magnetic Field," *Journal of Nonlinear Mathematical Physics*, vol. 32, no. 1, p. 2, Jan. 2025, <https://doi.org/10.1007/s44198-024-00250-9>
- [39] B. Gebhart, "Effects of viscous dissipation in natural convection," *J Fluid Mech*, vol. 14, no. 2, pp. 225–232, Oct. 1962, <https://doi.org/10.1017/S0022112062001196>
- [40] R. Cortell, "Viscous flow and heat transfer over a nonlinearly stretching sheet," *Appl Math Comput*, vol. 184, no. 2, pp. 864–873, Jan. 2007, <https://doi.org/10.1016/J.AMC.2006.06.077>
- [41] M. Subhas Abel, E. Sanjayanand, and M. M. Nandeppanavar, "Viscoelastic MHD flow and heat transfer over a stretching sheet with viscous and ohmic dissipations," *Commun Nonlinear Sci Numer Simul*, vol. 13, no. 9, pp. 1808–1821, Nov. 2008, <https://doi.org/10.1016/J.CNSNS.2007.04.007>
- [42] B. Ramandevi, J. V. R. Reddy, V. Sugunamma, and N. Sandeep, "Combined influence of viscous dissipation and non-uniform heat source/sink on MHD non-Newtonian fluid flow with Cattaneo-Christov heat flux," *Alexandria Engineering Journal*, vol. 57, no. 2, pp. 1009–1018, Jun. 2018, <https://doi.org/10.1016/j.aej.2017.01.026>
- [43] L. Anitha, B. J. Giresha, and M. L. Keerthi, "Irreversibility analysis of tangent hyperbolic fluid flow in a microchannel: a hybrid nanoparticles aspects," *Phys Scr*, vol. 98, no. 3, p. 035220, Mar. 2023, <https://doi.org/10.1088/1402-4896/acba53>
- [44] G. Bayou, E. Haile, and G. Awgichew, "Heat and mass flux dynamics of tangent hyperbolic nanofluid flow with unsteady rotatory stretching disk over Darcy-Forchheimer porous medium," *Phys Scr*, vol. 99, no. 12, p. 125206, Dec. 2024, <https://doi.org/10.1088/1402-4896/ad8972>
- [45] S. U. Khan, H. Waqas, S. A. Shehzad, and M. Imran, "Theoretical analysis of tangent hyperbolic nanoparticles with combined electrical MHD, activation energy and Wu's slip features: a mathematical model," *Phys Scr*, vol. 94, no. 12, p. 125211, Dec. 2019, <https://doi.org/10.1088/1402-4896/ab399f>
- [46] E. O. Fatunmbi, F. Mabood, H. Elmonser, and I. Tlili, "Magnetohydrodynamic nonlinear mixed convection flow of reactive tangent hyperbolic nano fluid passing a nonlinear stretchable surface," *Phys Scr*, vol. 96, no. 1, p. 015204, Jan. 2021, <https://doi.org/10.1088/1402-4896/abc3e9>
- [47] L. Reid, "An Introduction to Biomedical Computational Fluid Dynamics," 2021, pp. 205–222. https://doi.org/10.1007/978-3-030-76951-2_10

- [48] S. Sadighi, H. Afshar, M. Jabbari, and H. Ahmadi Danesh Ashtiani, "Heat and mass transfer for MHD nanofluid flow on a porous stretching sheet with prescribed boundary conditions," *Case Studies in Thermal Engineering*, vol. 49, p. 103345, Sep. 2023, <https://doi.org/10.1016/j.csite.2023.103345>
- [49] M. I. Khan, S. Qayyum, T. Hayat, M. I. Khan, A. Alsaedi, and T. A. Khan, "Entropy generation in radiative motion of tangent hyperbolic nanofluid in presence of activation energy and nonlinear mixed convection," *Phys Lett A*, vol. 382, no. 31, pp. 2017–2026, Aug. 2018, <https://doi.org/10.1016/j.physleta.2018.05.021>
- [50] R. Ali, M. R. Khan, A. Abidi, S. Rasheed, and A. M. Galal, "Application of PEST and PEHF in magneto-Williamson nanofluid depending on the suction/injection," *Case Studies in Thermal Engineering*, vol. 27, p. 101329, Oct. 2021, <https://doi.org/10.1016/j.csite.2021.101329>
- [51] N. Sher Akbar, A. Ebaid, and Z. H. Khan, "Numerical analysis of magnetic field effects on Eyring-Powell fluid flow towards a stretching sheet," *J Magn Magn Mater*, vol. 382, pp. 355–358, May 2015, <https://doi.org/10.1016/j.jmmm.2015.01.088>
- [52] A. M. Megahed, M. G. Reddy, and W. Abbas, "Modeling of MHD fluid flow over an unsteady stretching sheet with thermal radiation, variable fluid properties and heat flux," *Math Comput Simul*, vol. 185, pp. 583–593, Jul. 2021, <https://doi.org/10.1016/j.matcom.2021.01.011>
- [53] S. E. Waheed and A. M. Megahed, "Melting Heat Transfer Effects on Flow of a Micropolar Fluid with Heat Generation(Absorption) in Slip Flow Regime," *Applied Mathematics & Information Sciences*, vol. 16, no. 1, pp. 35–44, Jan. 2022, <https://doi.org/10.18576/amis/160104>
- [54] J. Peddieson, *Boundary Layer Theory for a Micropolar Fluid*. Virginia Polytechnic Institute, 1968.
- [55] J. V. Tawade, C. N. Guled, S. Noeiaghdam, U. Fernandez-Gamiz, V. Govindan, and S. Balamuralitharan, "Effects of thermophoresis and Brownian motion for thermal and chemically reacting Casson nanofluid flow over a linearly stretching sheet," *Results in Engineering*, vol. 15, p. 100448, Sep. 2022, <https://doi.org/10.1016/j.rineng.2022.100448>

Nomenclature

Symbol	SI Unit	Description
A_0		Rate of stretching surface
B_0	$A\ m^{-1}$	Magnetic field strength
c_p	$J/kg\ K$	Specific heat
M	T	Magnetic field vector
f		Dimensionless stream function
Pr		Prandtl number
C_w	<i>mole</i>	Concentration of nanoparticles at the surface
C_∞	<i>mole</i>	Ambient concentration of nanoparticles
U_w	ms^{-1}	Velocity at the wall
S		Suction and injection parameter
$\theta(\eta)$		Dimensionless temperature
$g(\eta)$		Dimensionless concentration
Nt		Thermophoretic parameter
Nb		Brownian motion
T_w	K	Temperature of Surface
T_∞	K	Surrounding temperature
Sc		Schmidt number

D_B	$m^2 s^{-1}$	Brownian diffusion coefficient
D_T	$m^2 s^{-1}$	Thermophoresis diffusion coefficient
ρ_c	$Jm^{-3}K^{-1}$	Heat capacity of nanfluid
Re_x	$Kg m^{-3}$	Local Reynolds number
n		Power law index
f'		Dimensionless velocity
η		Similarity variable
σ	Sm^{-1}	Electrical conductivity
Γ		Positive time constant
α	$m^2 s^{-1}$	Thermal diffusivity
ρc_p	$Jm^{-3}K^{-1}$	Heat capacity of nanoparticles
ν	$m^2 s^{-1}$	Kinematic viscosity
ρ	$kg m^{-3}$	Density
We		Weissenberg number
w		Condition at the surface
∞		Condition at the free stream
(u, v)	$m s^{-1}$	Velocity Component
(x, y)	m	Coordinate Axes